doi:10.1016/j.jmb.2005.09.099 J. Mol. Biol. (2006) 356, 9–21

JMB

Available online at www.sciencedirect.com

SCIENCE DIRECT®

ELSEVIER

Crystal Structure of the *S. cerevisiae* Exocyst Component Exo70p

Zsuzsa A. Hamburger[1], Agnes E. Hamburger[2], Anthony P. West Jr[2] and William I. Weis[1]*

[1]*Departments of Structural Biology and Molecular & Cellular Physiology, Stanford University School of Medicine Stanford, CA 94305-5126 USA*

[2]*Division of Biology 114-96 California Institute of Technology, Pasadena, CA 91125 USA*

**Corresponding author*

The exocyst is an evolutionarily conserved multiprotein complex required for the targeting and docking of post-Golgi vesicles to the plasma membrane. Through its interactions with a variety of proteins, including small GTPases, the exocyst is thought to integrate signals from the cell and signal that vesicles arriving at the plasma membrane are ready for fusion. Here we describe the three-dimensional crystal structure of one of the components of the exocyst, Exo70p, from *Saccharomyces cerevisae* at 3.5 Å resolution. Exo70p binds the small GTPase Rho3p in a GTP-dependent manner with an equilibrium dissociation constant of approximately 70 μM. Exo70p is an extended rod approximately 155 Å in length composed principally of alpha helices, and is a novel fold. The structure provides a first view of the Exo70 protein family and provides a framework to study the molecular function of this exocyst component.

Keywords: exocyst; exocytosis; membrane trafficking; protein structure

Introduction

The exocyst, also known as the Sec6/8 complex in mammals, is an evolutionarily conserved eight-protein complex required for the targeting and tethering of post-Golgi vesicles to the plasma membrane.[1,2] The exocyst is composed of the proteins Sec3, Sec5, Sec6, Sec8, Sec10, Sec15, Exo70 and Exo84. In yeast, mutations in the exocyst lead to defects in exocytosis and arrest growth of the daughter cell.[3,4] Exocyst mutants accumulate post-Golgi secretory vesicles in the cytoplasm due to defects in tethering vesicles to the plasma membrane.[4,5] The exocyst complex works upstream of the soluble NSF attachment protein receptor proteins (SNAREs) required for membrane fusion. The *Saccharomyces cerevisiae* exocyst may regulate SNARE complex assembly through its interaction with Sec9, Sro7 and Sro77.[6,7] Unlike SNARE proteins, which have a relatively uniform membrane distribution,[8] the exocyst localizes to specific sites on cellular membranes.[3,9–11] The exocyst is therefore believed to target vesicles to specific sites on the plasma membrane. In addition to its role in spatially restricting exocytosis, the exocyst has also been shown to influence filpodia formation, tubulin polymerization, protein synthesis and pre-mRNA splicing.[12–15]

A number of GTPases, including members of the Rho, Ral and Rab families, have been shown to associate with the exocyst, leading to the theory that the function of the exocyst is to integrate signals from the cell that indicate that the arriving vesicles are ready to fuse with the plasma membrane.[16,17] In particular, Rho GTPases regulate organization of the cytoskeleton, suggesting that the exocyst coordinates communication between vesicles and changes in the cytoskeleton required for membrane trafficking. In yeast, Rho3p directs delivery of transport vesicles to sites of exocytosis by binding to Exo70p,[18,19] while Rho1 and Cdc42 direct proper localization of the exocyst by binding to Sec3p.[3,20] The Rab protein Sec4 regulates the exocyst through its interaction with Sec15.[21] In mammalian cells, RalA binds to both Sec5 and Exo84. This dual interaction is thought to regulate assembly of the complex.[22–24] Mammalian Exo70 interacts with the GTPase TC10, and translocates to the plasma membrane in response to insulin.[25]

Recent work indicates that the exocyst is not found exclusively as a single protein complex in the cell. Sub-complexes of exocyst components, as well as some of the individual subunits, appear to have specific functions.[5,14,26–29] For example, yeast Sec3p

Abbreviations used: SNAREs, NSF attachment protein receptor proteins; MAD, multiwavelength anomalous dispersion; rmsd, root-mean-squared difference; MALS, multiangle light scattering; WT, wild-type; TEV, tobacco etch virus; SPR, surface plasmon resonance.

E-mail address of the corresponding author: bill.weis@stanford.edu

0022-2836/$ - see front matter

directs assembly of the exocyst at sites of membrane fusion by binding directly to the plasma membrane at the bud tip.[9,30] This interaction is independent of the actin cytoskeleton as well as the presence of the other members of the exocyst,[3] but is dependent on interaction with Rho proteins.[20,31] Interestingly, the Rho-binding domain is absent in mammalian Sec3 orthologs, whereas mammalian Exo70 appears to interact with membranes, and is an important determinant of cell polarity.[32]

Few biochemical data on the molecular interactions of Exo70 are available. The N-terminal region of Exo70 (residues 1–384) binds Sec8 and TC10, whereas the C-terminal region (residues 385–653) is important for localization to the membrane possibly through interactions with another protein.[25] The C-terminal 385 residues of *S. cerevisiae* Exo70p binds Rho3p both in yeast two-hybrid as well as in pull-down assays.[18,19] Genetic interactions between Rho3p and Exo70p have also been identified in *Schizosaccharomyces pombe*, although physical interaction between the two proteins has not been confirmed in this case.[33] Thus, yeast Exo70p may be a key exocyst component required for coordinating vesicle targeting with changes in the cytoskeleton. Mammalian Exo70 also binds to BIG2, a guanine nucleotide-exchange protein that regulates transport of proteins from the Golgi apparatus to the cell surface.[34] Exo70 has also been shown to modulate microtubule dynamics by inducing microtubule depolymerization, but the molecular basis of this activity is not known.[13]

Here we present the crystal structure of Exo70p from *Saccharomyces cerevisiae* at 3.5 Å resolution. Binding studies show a surprisingly weak, GTP-dependent interaction between Exo70p and Rho3p. This study provides the first molecular view of the Exo70p protein family and provides a framework to study the function of this exocyst component at a molecular level.

Results and Discussion

Overall structure and domain organization

Exo70p from *S. cerevisiae* was expressed in *Escherichia coli* and purified. Initial attempts to crystallize full length Exo70p failed. Purified Exo70p that was stored at 4 °C for several weeks degraded into two smaller fragments. These fragments were purified and their N and C termini identified by N-terminal sequencing and mass spectrometry. Both fragments

Table 1. Crystallographic data processing and refinement statistics

Exo70p construct	63–524	63–524	63–524	63–624
Cell dimensions		$a=134.54$ Å $c=124.16$ Å		$a=415.73$ Å $b=55.13$ Å $c=132.93$ Å $\beta=104.05°$
Space group	$P3_212$	$P3_212$	$P3_212$	$C2$
Wavelength	0.97950 (peak)	0.97963 (inflection)	0.9393 (remote)	0.9796 (peak)
Resolution	20–3.3	20–3.3	20–3.5	20–3.5
No. measured refl.	93,687	93,883	78,608	99,085
No. unique refl.	18,839	18,865	15,796	36,080
Completeness (%)[a]	97.5 (98.3)	97.5 (98.3)	97.2 (98.3)	95.0 (92.0)
I/σ	13.2 (2.8)	19.9 (2.5)	19.7 (3.2)	12.6 (3.0)
R_{merge}[b]	0.077 (0.541)	0.060 (0.599)	0.063 (0.453)	0.076 (0.354)
Refinement				
Resolution (Å)		20.0–3.5		
Reflections in working set		33,729		
Reflections in test set		2175		
Average B (Å^2)		129.2		
Overall anisotropic B (Å^2)				
B_{11}		−11.8		
B_{13}		40.7		
B_{22}		15.1		
B_{33}		−3.4		
Number of non-hydrogen protein atoms		4153		
R_{free} (%)[c]		30.5		
R_{cryst} (%)[d]		25.4		
rms deviations from ideality				
Bond lengths (Å)		0.007		
Bond angles (deg.)		1.19		
Ramachandran plot				
% in most favored regions		83.4		
% in additional allowed regions		15.8		

Values in parentheses represent the highest resolution shell.

[a] Complete = (number of independent reflections)/total theoretical number.

[b] $R_{merge}(I) = (\Sigma|I(i) - \langle I(h)\rangle|/\Sigma I(i))$, where $I(i)$ is the ith observation of the intensity of the hkl reflection and $\langle I\rangle$ is the mean intensity from multiple measurements of the h,k,l reflection. $R_{cryst}(F) = \sum_h ||F_{obs}(h)| - |F_{calc}(h)||/\sum_h |F_{obs}(h)|$, where $|F_{obs}(h)|$ and $|F_{calc}(h)|$ are the observed and calculated structure factor amplitudes for the h,k,l reflection.

[c] R_{free} is calculated over reflections in a test set not included in the refinement.[61]

[d] $R_{cryst}(F) = \sum_h ||F_{obs}(h)| - |F_{calc}(h)||/\sum_h |F_{obs}(h)|$, where $|F_{obs}(h)|$ and $|F_{calc}(h)|$ are the observed and calculated structure factor amplitudes for the h,k,l reflection.

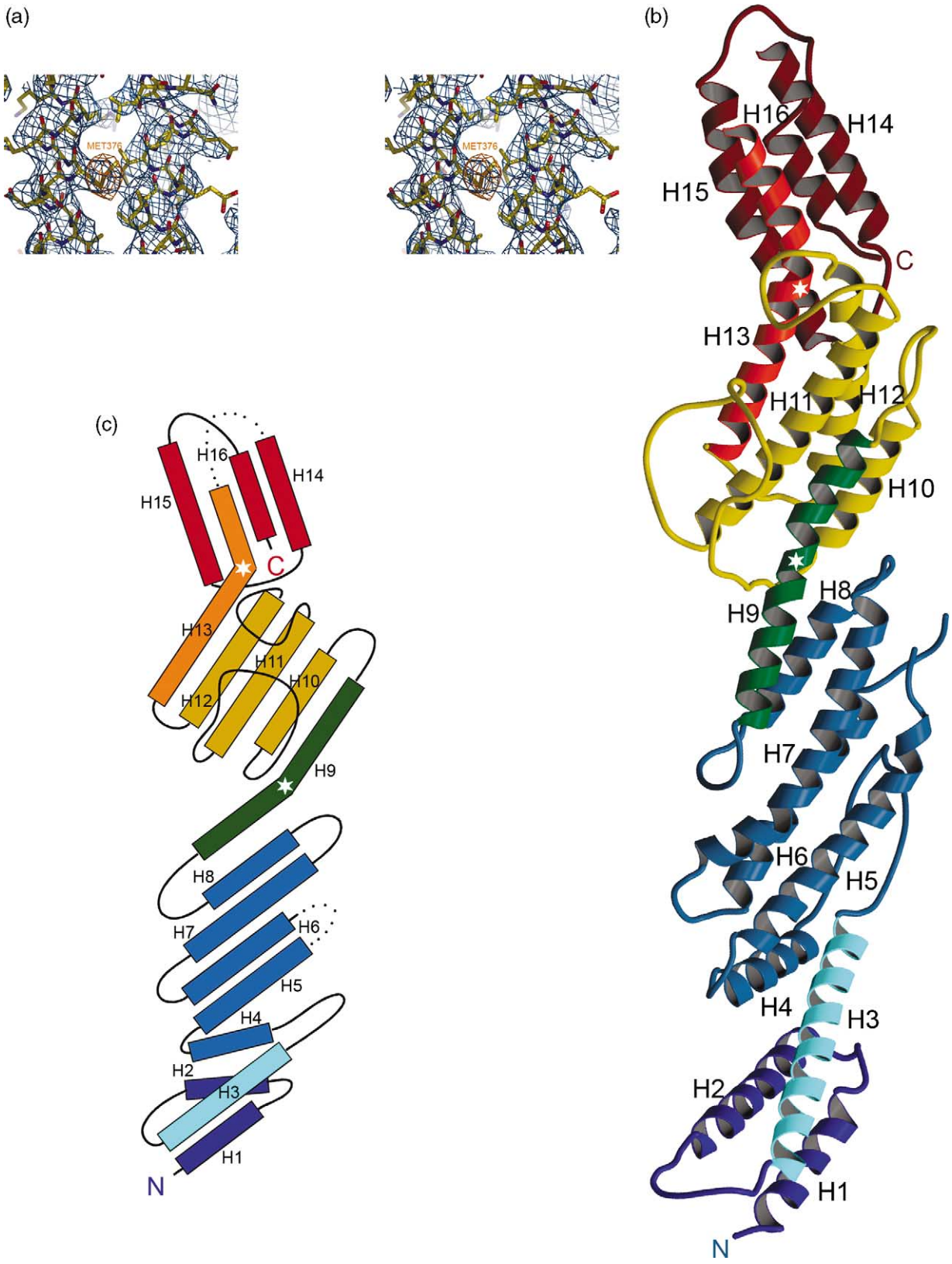

Figure 1. Crystal structure of Exo70p. (a) Stereo view of the Exo70p model superimposed on a 3.5 Å. σ_A weighted[47] $2F_o - F_c$ electron density map contoured at 1.0 σ shown in blue. An anomalous Fourier map contoured at 4σ and corresponding to selenium positions is shown in orange. (b) Ribbon diagram of the structure of *S. cerevisiae* Exo70p. Domain 1 is colored blue, domain 2 is colored yellow and domain 3 is colored red. Helices H1 and H2 are colored sky blue while H3 is colored cyan to indicate that this region of Exo70p could be assigned as a separate subdomain. The helix (H9) connecting domains 1 and 2 is colored green while the helix (H13) connecting domains 2 and 3 is colored orange. White stars represent the kink found in these helices. N and C termini are labeled. (c) Topology diagram for Exo70p. The same color scheme is used as in (b). Loops disordered in the crystal are represented as dotted lines.

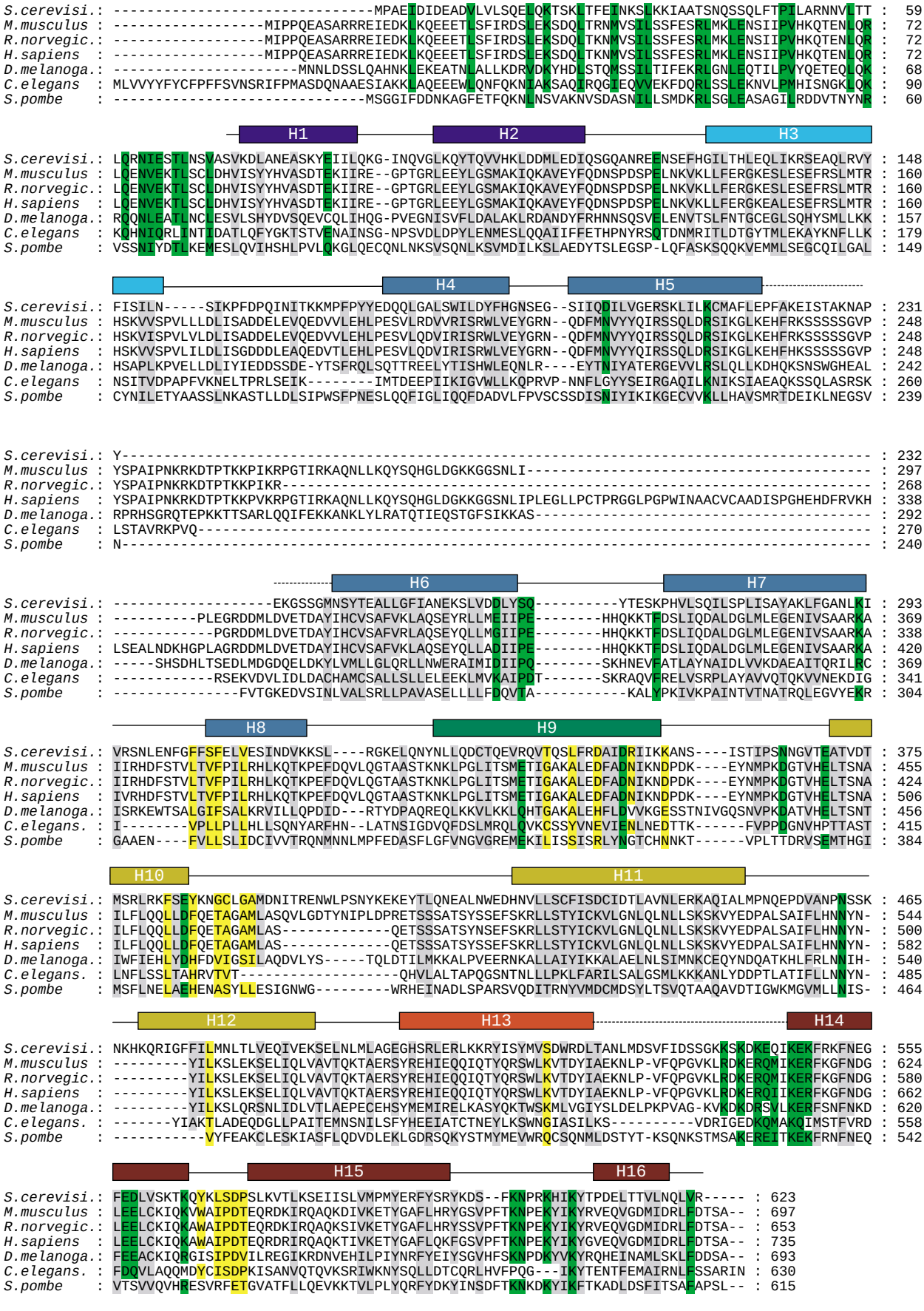

Figure 2 (*legend on opposite page*)

were subcloned, expressed, purified, and crystallized. The smaller Exo70p proteolytic fragment, comprising residues 63–524, crystallized in the trigonal space group $P3_212$, with two molecules in the asymmetric unit (Table 1). The best crystal, grown from selenomethionine-substituted protein, diffracted X-rays to 3.3 Å resolution. The structure was solved by multiwavelength anomalous dispersion (MAD) phasing (Figure 1(a)). The longer fragment, which also starts at residue 63 but extends to the native C terminus (residue 623), crystallized in the monoclinic space group *C*2. The monoclinic crystals contain four independent copies in the asymmetric unit, and diffracted X-rays to 3.5 Å (Table 1). The relatively low-resolution diffraction and the presence of 56 selenomethionine sites prevented determination of the structure by MAD phasing, and the structure was solved by molecular replacement using the refined structure of the 63–524 fragment as a search model (Figure 1(a)). The final model contains residues 73–223, 236–527 and 544–623, and is therefore the most complete model of an exocyst subunit to date. Residues 63–72, 224–235, and 528–543 are not visible in the electron density map and are presumably disordered.

Exo70p has an elongated structure with overall dimensions of ~155 Å × 35 Å × 35 Å (Figure 1(b) and (c)). The structure is composed principally of α-helices (65%), and can be divided into three domains (Figure 1(b)) based upon the overall arrangement of helices, inter-domain hinge points, and proteolytic sensitivity. Domain 1 (D1) of Exo70p (residues 73–341) comprises helices H1–H8 and the N-terminal portion of H9 (Figure 1(b)). This region is a continuous set of antiparallel helices that pack together to form an elongated structure. The last helix, H9, is noticeably bent, with its N-terminal portion packed against the preceding helices. Many of the helices are staggered such that a portion of one face that would normally pack against an adjacent helix is instead exposed to solvent, or is packed against extended loops. For example, the loop spanning residues 157–176 between H3 and H4 makes extensive, mostly hydrophobic, contacts with H5 and H6. The residues buried between the helices are mostly hydrophobic with a notable exception: Arg206 of H5 forms polar interactions with Glu253 of H6, as well as Tyr174. Residues 206 and 253 are conserved in Exo70 proteins from different species (Figure 2) and likely play a role in protein folding and stability.

The assignment of the first nine helices to a single domain is somewhat arbitrary, and other, equally valid divisions can be made. For example, the first three helices of D1 form a three-helix bundle that angles away slightly from the remainder of the domain (shown in sky blue and cyan in Figure 1(b)), and could therefore be considered a separate subdomain. On the other hand, the relatively short H4 partially packs against this bundle, and is canted away from H5, so the first four helices could also be considered to be a subdomain. Given that there is no obvious dividing point and that the helices form a continuously packed unit, we have chosen to assign these elements to a larger, single domain. This is also consistent with the lack of hinge flexibility or proteolytic sensitivity within this region (see below).

Domain 2 (D2) (residues 342–514) comprises the portion of H9 C-terminal to the kink (green helix, Figure 1(b) and (c)) and H10–H13. Similar to H9, H13 is bent, and its N-terminal portion forms part of D2, while its C-terminal portion begins the next domain (orange helix, Figure 1(b) and (c)). D2 is an unusual structure in which the four helices H9, H10, H12, and H13 form a semicircular "blanket" around the largely hydrophobic H11. The other side of H11 is buried by large loops that connect H10 to H11, and H11 to H12. The H10-H11 loop, residues 384–423, bends back against the molecule to form extensive hydrophobic and hydrophilic contacts with H10, H11 and H12. The loop between H11 and H12 (residues 451–469) forms predominantly hydrophilic interactions with H11, H12, and H13. Apart from a single hydrogen bond between Lys409 and Asn460, no direct bonds are found between the two extended loops.

Proteolysis of Exo70p defines domain 3 as residues 515–623. The structure consists of the C-terminal end of the bent H13, and H14–16. The four helices form a hydrophobic core, one end of which is unusually rich in aromatic residues. This domain can be expressed and purified as an independent folding unit, consistent with its release from the rest of Exo70p by proteolysis (data not shown).

Comparison to other protein structures

Neither the complete model of Exo70p nor the individual regions display significant similarity to known structures, as assessed by structural similarity searches in DALI.[35] The top matches were the heat shock cognate protein 71 kDa fragment (pdb code 1hx1, $Z = 6.9$, rmsd = 2.5 Å, over 77 residues, 10% sequence identity); importin beta subunit (pdb code 1qgr, $Z = 6.2$, rmsd = 2.6 Å, over 86 residues, 6% sequence identity); alginate lyase A1-III (pdb code 1qaz, $Z = 6.1$, rmsd = 7.1 Å, over 152 residues,

Figure 2. Structure-based sequence alignment of Exo70. Exo70 from seven different species were aligned in CLUSTALX[60] using secondary structure information in the profile alignment. Strongly and moderately conserved surface-exposed residues are highlighted in dark and light green, respectively. Residues that form the core of the Exo70p domains and are conserved across species are highlighted in gray. Yellow denotes residues that are conserved and form the interdomain interfaces. Crystallographically determined secondary structure elements are shown above the sequences and are colored as in Figure 1(b). Loops disordered in the crystal are represented as dotted lines.

7% sequence identity); and chromosome partition protein mukf (pdb code 1t98, $Z=5.2$, rmsd = 14.1 Å, over 119 residues, 8% sequence identity). All of these proteins are helical, and any local similarities between portions of these proteins and Exo70p likely reflect packing common to most helix–helix interactions. Thus, it appears that Exo70p possesses a novel fold.

Molecular flexibility and oligomeric state

The individual domains are nearly identical among the four molecules of the asymmetric unit, but the angle between domains 1 and 2 differs, due to a bend in H11 at residue Gln342 (Figure 3). When domains 1 from molecules A and D are superimposed, the angle formed between domain 2 of A and domain 2 of D is 14.6°. In contrast, the angle between domains 2 of molecules B and D is 4.3°, and is 8.9° between molecules C and D. Although there is variation in the angle between domains 1 and 2, the surface area buried between them is very similar amongst the four different molecules in the asymmetric unit (1108 Å^2 for molecule A, 1148 Å^2 for molecule B, 1109 Å^2 for molecule C and 1146 Å^2 for molecule D). The surface area buried between domains 2 and 3 is comparable, ~1350 Å^2 in the four crystallographically independent copies, but unlike the D1–D2 interface no flexibility in the relative positions of D2 and D3 is apparent. The D1–D2 and D2–D3 interfaces are both predominantly hydrophobic, and are particularly rich in aromatic amino acids.

The same dimer of Exo70p was found in both the monoclinic and trigonal crystals. In both cases, a crystallographic 2-fold axis relates the two protomers. The dimer interface is made by the interaction of H1 from one protomer with the extended loop structure found in domain 1 (residues 157–176) of the second protomer (Figure 4(a)). The Exo70p construct 63–623 (monoclinic crystal form), which has an expected molecular mass of 64 kDa, elutes from a gel filtration column with an apparent molecular mass of ~80 kDa (Figure 4(b), upper panel). The extended structure of Exo70p probably contributes to the larger-than-expected molecular mass observed in the gel filtration experiments. The construct was confirmed to be monomeric in solution using multiangle light scattering (MALS) (data not shown). The full length Exo70p protein (residues 1–623) is also monomeric in solution as assessed by gel filtration chromatography. The protein elutes with an apparent molecular mass of ~110 kDa as compared to the expected molecular mass of 72 kDa (Figure 4(a), upper panel). Again, the extended structure of the molecule probably contributes to the apparent molecular mass. These results suggest that the 2-fold symmetric dimer present in the crystals is due to crystal packing and is unlikely to be functionally important. However, the 2240 Å^2 of surface area buried in this interface is significantly higher than the average surface area buried in non-specific crystal contacts (570 Å^2).[36]

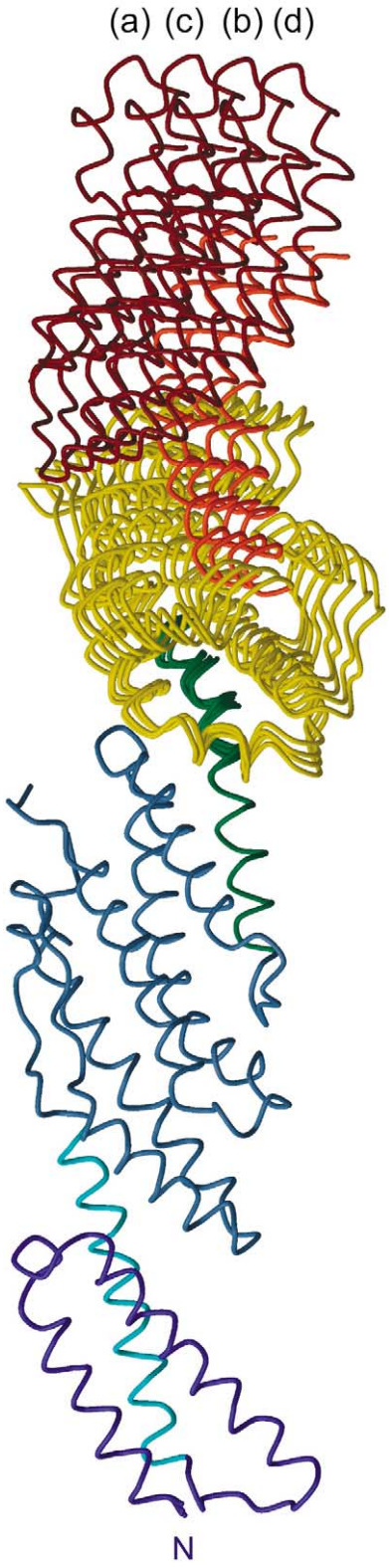

Figure 3. Exo70p flexibility. C^{α} atoms of domain 1 of each of the four molecules in the *C*2 asymmetric unit were superimposed to illustrate the flexibility seen in Exo70p. The same color scheme is used as in Figure 1(b). The N terminus is labeled. (a), (b), (c), (d) Refer to the four molecules found in the asymmetric unit of the *C*2 crystals (construct 63–623).

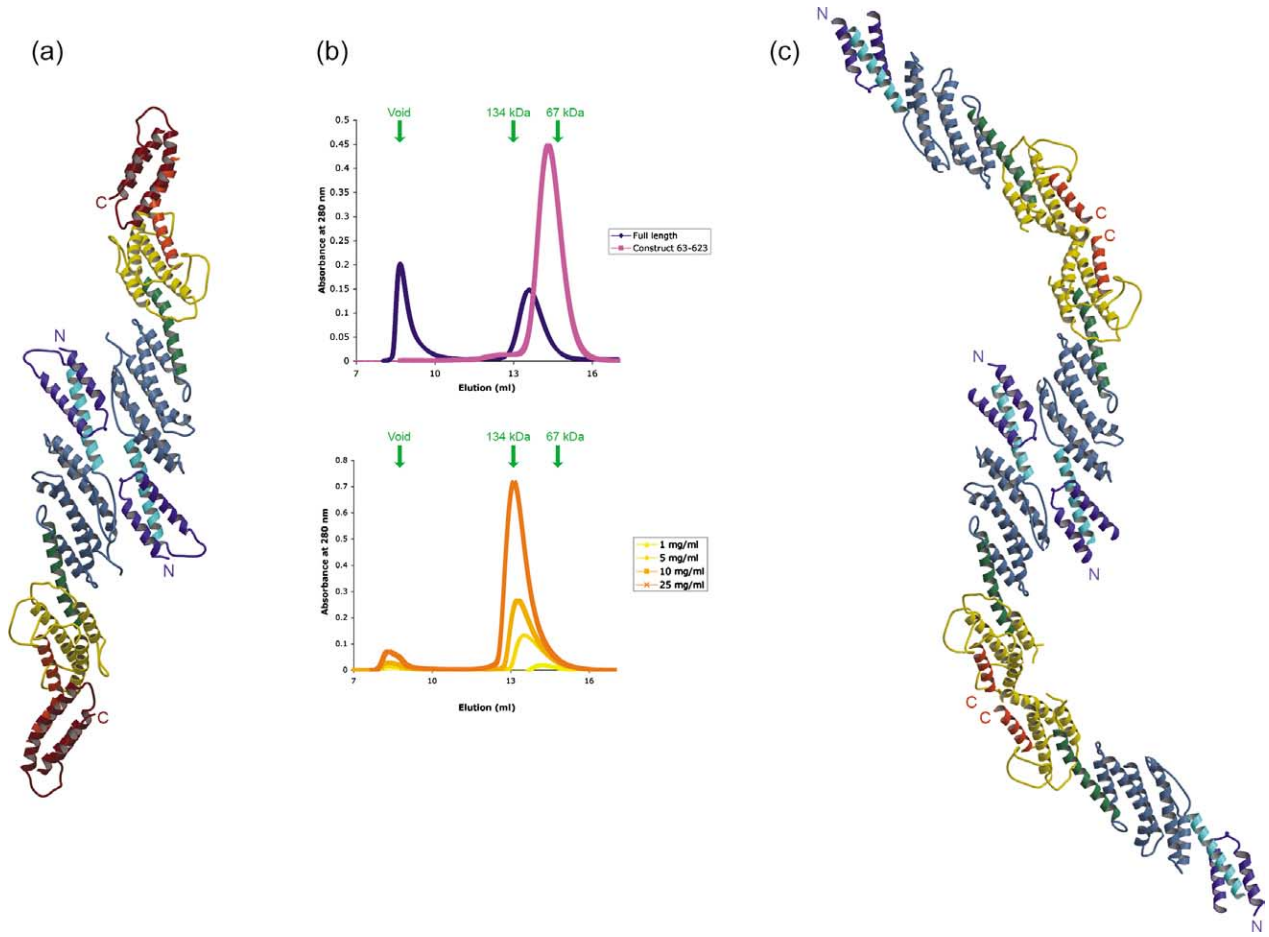

Figure 4. Exo70p dimerization. (a) Ribbon diagram of the Exo70p dimer seen in the monoclinic crystal form. The same color scheme is used as in Figure 1(b). N and C termini are labeled. (b) Gel filtration chromatography shows that full length Exo70p and construct 63–623 are monomeric in solution (top panel), whereas construct 63–524 exhibits concentration-dependent dimerization (bottom panel). (c) Ribbon diagram of the Exo70p dimers seen in the trigonal crystal form. The same color scheme is used as in Figure 1(b). N and C termini are labeled.

This indicates that this surface has features that are favorable for protein–protein interactions and may be utilized both for crystal packing as well as for ligand binding by Exo70p.

In contrast to the Exo70p constructs that extend to residue 623, the fragment that arises from proteolysis of the domain 2–3 interface, residues 63–524 (trigonal crystal form), exhibits concentration-dependent dimerization, as shown by gel filtration (Figure 4(b), lower panel) and MALS (data not shown). This dimer is functionally not relevant as it likely forms at the C-terminal region of the protein at the hydrophobic interface between domains 2 and 3 that is exposed when domain 3 is removed from the construct. This dimer is seen in the trigonal crystals (Figure 4(c)).

The surface of Exo70p contains hydrophilic, hydrophobic and charged regions that may be important for interactions with regulatory proteins, other exocyst components, or membranes (Figure 5(a)). Residues Phe216, Phe220, Ile293, Phe301 and Val622 are exposed on the surface of Exo70p. With the exception of Val622, these residues are generally not conserved in other species and may be important for a function of Exo70p specific to *S. cerevisiae* (Figure 2).

Comparison with other Exo70 sequences

An alignment of Exo70 amino acid sequences from seven species, including two yeast, worm, fly, rat, mouse and human, is presented in Figure 5. Surface-exposed residues that are 100% conserved are shown in dark green while less well (>80%) conserved, surface-exposed residues are shown in light green. Buried residues that form the core of the three domains are for the most part conserved or replaced with residues whose side-chains are compatible with burial in the core (gray in Figure 5). Residues that mediate packing between domains are less conserved (yellow in Figure 5), suggesting that the relative positions of the domains, and/or the inter-domain flexibility, may vary among Exo70p orthologs.

The conserved surface-accessible residues can be seen in Figure 5(b). The last 100 residues of Exo70p, corresponding to domain 3, contain a number of highly conserved, solvent-exposed charged

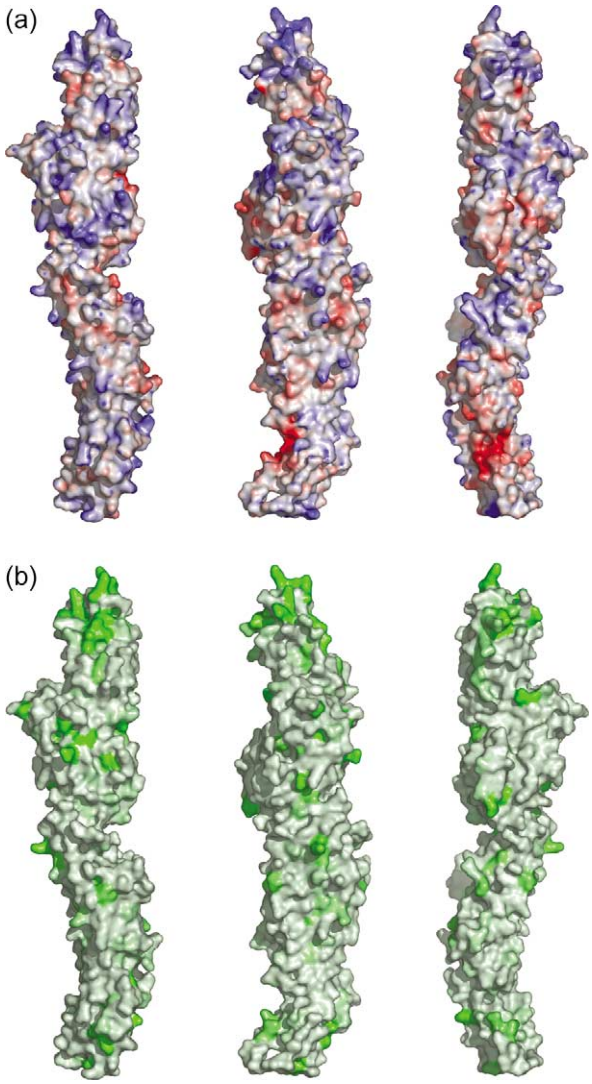

Figure 5. Molecular surface representations of Exo70p. The three views are successive 90° rotations around a vertical axis with the N termini pointing toward the bottom. (a) The electrostatic surface potential for Exo70p is shown. Blue and red represent regions of positive and negative electrostatic potential, respectively, contoured at $\pm 8k_BT/e$. (b) Surface of Exo70p colored according to sequence conservation based on an alignment from seven organisms. Highly conserved residues are bright green and semi-well conserved residues are light green.

residues (Figures 2(b) and 5). This region of the protein is thought to be important for membrane localization possibly through interaction with other proteins.[25] In addition, the presence of numerous positively charged lysine residues present in a loop at the tip of Exo70p (toward the C-terminal side) suggests that this region of the protein may mediate membrane association by binding to acidic phospholipids.

GTP-dependent, weak binding to Rho3p

The interaction between Exo70p and Rho3p was previously investigated using yeast two-hybrid and pull-down assays.[18,19] Although these techniques were valuable for identifying Exo70p as an effector for Rho3p, they did not provide information about the affinity between the two proteins. Surface plasmon resonance was used to determine the binding affinity between Rho3p and Exo70p. Rho3p, both wild-type (WT) and the constitutively active, non-hydrolyzing mutant Q74L,[37] were expressed and purified from *E. coli*. To enable higher expression levels, the C-terminal CAAX boxes needed for fatty acylation were removed in the Rho3p constructs. As reported,[18] the interaction between Exo70p and WT-Rho3p is GTP-dependent, as binding was greatly reduced when GTP was replaced with GDP in the running buffer (Figure 6(a)). In order to determine the equilibrium dissociation constant K_D for the Exo70p–Rho3p interaction, increasing concentrations of Exo70p were injected over immobilized Rho3p. During the course of the concentration series, the GTP present in the running buffer non-specifically hydrolyzed to GDP at room temperature, reducing the interaction and preventing determination of an accurate K_D. When fresh GTP buffer was added back into the running buffer, binding response immediately increased, showing that the protein molecules were not otherwise compromised during the experiment (data not shown). To eliminate complications arising from the non-specific hydrolysis of GTP, the non-hydrolyzing Rho3p-Q74L mutant was used to determine the K_D values for various Exo70p constructs. However, because complete nucleotide exchange was not achieved, the measured affinities may be slightly understimated.

Full length Exo70p binds to Rho3-Q74L with an equilibrium dissociation constant (K_D) of 70 μM (Figure 6(b)). The K_D for the binding between Rho3p-Q74L and Exo70p construct 63–623 is 30 μM (Figure 6(c)). The Exo70p construct 63–524 also binds to Rho3p-Q74L (data not shown), but the K_D for the interaction could not be determined because binding was not saturated at the highest concentration of protein achievable. The interaction is surprisingly weak compared to other small GTPase–substrate interactions, which typically fall in the nanomolar range of K_D. There are several possible reasons for the low affinity observed between Exo70p and Rho3p. First, in the cell both Exo70p and Rho3p are associated with membranes. It is possible that the restriction to the two dimensions of a membrane effectively increases the interaction, which otherwise appears exceptionally weak when studied in free solution. Second, post-translational modifications of one or both partners might strengthen their affinity, although no evidence exists for this possibility. A third, and more intriguing, scenario is that the functional interaction of Rho3p with the exocyst requires not only Exo70p, but also one or more other subunits. Future experiments will be required to assess these possibilities. Nonetheless, the present structure provides a strong foundation

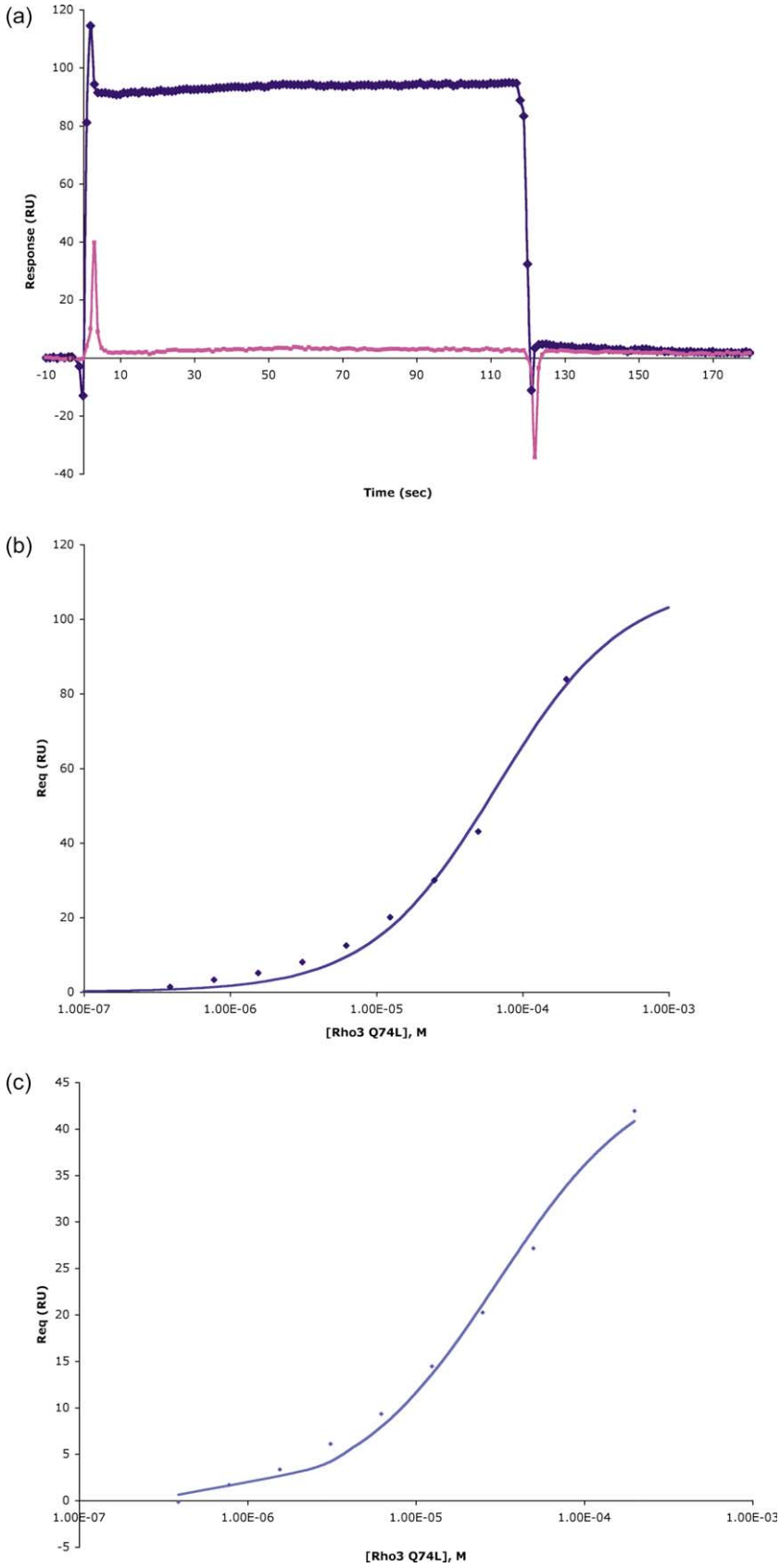

Figure 6. Biosensor analyses of Rho3p binding to Exo70p. (a) Sensorgram from binding experiments in which 40 μM of Rho3p was injected over Exo70p construct 63–623 in the presence of GTP (blue) or GDP (pink). (b) and (c) Equilibrium binding response (R_{eq}) *versus* the log of concentration is shown for biosensor experiments in which the activated mutant Rho3p-Q74L was injected over full length Exo70p (b) or the Exo70p construct 63–623 (c) immobilized on a biosensor chip. Best-fit binding curve based on a 1:1 binding model is superimposed on the binding data. K_D could not be derived for construct 63–524 because the binding curve could not be saturated at the highest possible concentration tested (data not shown).

for further studies of Exo70 function and mechanism.

Materials and Methods

Protein expression and purification

Constructs encoding amino acid residues 1–632, 63–623 or 63–524 of Exo70p with an N-terminal six-histidine tag followed by a linker and a tobacco etch virus (TEV) protease site were subcloned into the pProExHTb bacterial expression vector (Life Technologies). BL21 RIL+ cells transformed with the Exo70p construct were grown in Luria-Bertani (LB) broth to an A_{600} of 0.6, then induced for 2 h at 25 °C with 1 mM IPTG. Cells were harvested by centrifugation and lysed by French press. The six-histidine tagged Exo70p was purified by Ni-NTA chromatography (Qiagen) followed by size-exclusion chromatography on a Superdex 200 gel filtration column (GE Healthcare) in 50 mM Tris (pH 8), 300 mM NaCl, 2 mM DTT, 1 mM EDTA. Peak fractions were pooled, concentrated and subjected to TEV cleavage overnight at 4 °C. The cleaved protein was loaded onto a 2 ml Ni-NTA column to remove uncleaved sample and then loaded onto a Mono Q column (GE Healthcare) equilibrated with buffer A (50 mM Tris (pH 8), 2 mM DTT, 1 mM EDTA). A linear gradient was applied from buffer A to buffer A + 0.5 M NaCl to elute the protein from the column. Peak fractions were pooled and loaded onto a Superdex 200 gel filtration column (GE Healthcare) in buffer A + 300 mM NaCl. The purified Exo70p protein was concentrated to 30 mg/ml and stored at 4 °C.

Selenomethionine-substituted versions of Exo70p constructs 63–623 and 63–524 were produced as described[38] and purified under the same conditions as the native protein. Amino acid composition analysis showed ~100% replacement of the methionine residues by selenomethionine (data not shown).

A construct encoding WT-Rho3p lacking the C-terminal four residues corresponding to the CAAX box, with an N-terminal six-histidine tag followed by a linker and a TEV protease site was subcloned into the pProExHTb bacterial expression vector (Life Technologies). The Rho3p-Q74L single mutant was made subsequently using the QuikChange mutagenesis protocol (Stratagene). BL21 RIL+ cells transformed with the Rho3p constructs were grown to an A_{600} of 0.6 in LB and induced for 2 h at 25 °C with 1 mM IPTG. Cells were harvested by centrifugation and lysed by French press. The six-histidine tagged constructs were purified by Ni-NTA chromatography (Qiagen) in the presence of 5 mM $MgCl_2$. Size-exclusion chromatography on a Superdex 200 gel filtration column (GE Healthcare) in 50 mM Hepes (pH 7.5), 150 mM NaCl, 2 mM DTT, 5 mM $MgCl_2$ was used for further purification. Peak fractions were pooled and the protein was concentrated to 5 mg/ml and stored at 4 °C.

Crystallization and data collection

Selenomethionine-substituted protein crystals of the Exo70p construct 63–524 (space group $P3_212$, $a=b=134.54$ Å, $c=124.16$ Å; two molecules per asymmetric unit) were grown at 22 °C in sitting drops by combining 1 μl of protein solution (5 mg/ml in 50 mM Tris (pH 8), 300 mM NaCl, 2 mM DTT, 1 mM EDTA) with 1 μl of precipitant solution (20% (w/v) PEG 3350, 0.3 M K_2SO_4). Before data collection, crystals were transferred to a cryoprotectant solution (22% PEG 3350, 0.2 M K_2SO_4, 20% (v/v) glycerol). A multiwavelength anomalous dispersion (MAD) data set to 3.3 Å, using crystals from selenomethionine substituted Exo70p, was measured at the Advanced Light Source (ALS, Berkeley, CA) beamline 5.0.2.

Selenomethionine substituted protein crystals of the Exo70p construct 63–623 (space group $C2$, $a=415.73$ Å, $b=55.13$ Å, $c=132.93$ Å, $\beta=104.05°$; four molecules per asymmetric unit) were grown at 22 °C in hanging drops by combining 1 μl of protein solution (7 mg/ml in 50 mM Tris (pH 8), 300 mM NaCl, 2 mM DTT, 1 mM EDTA) with 1 μl of precipitant solution (0.1 M Mes (pH 6.1), 20% PEG 20,000, 0.2 M Mg_2CH_3COO). Before data collection, crystals were transferred to a cryoprotectant solution (0.1 M Mes (pH 6.1), 20% PEG 20,000, 0.2 M Mg_2CH_3COO, 20% ethylene glycol) and cryo-preserved. A single wavelength anomalous diffraction (SAD) data set to 3.5 Å was measured at ALS beamline 8.3.1.

Structure determination and phasing

Data were processed and scaled with the HKL package.[39] Twenty of the potential 22 selenium sites of the selenomethionine substituted 63–524 construct were identified by SOLVE.[40] Heavy-atom refinement and phasing were performed with the program SHARP,[41] yielding phases to 3.5 Å with a mean figure of merit of 0.445. An initial MAD electron density map was calculated to 3.5 Å and solvent flattened using Solomon[42] as implemented in SHARP.[41] A skeleton of the map[43] served as a starting point for model building using the program O.[44] Map interpretation was aided by an anomalous Fourier map that allowed identification of methionine residues that were used as markers for the assignment of the rest of the sequence. Refinement was carried out on the peak wavelength dataset using the simulated annealing, energy minimization and group temperature (B) factor protocols in CNS[45] with bulk solvent, anisotropy corrections, and NCS restraints. The test set of reflections for calculating R_{free} was generated with the thin shell method in DATAMAN.[46] The NCS operator was broken into two operators covering domain 1 (residues 75:114, 130:220, 239:342; force constant = 300 kcal/mol Å^2) and domain 2 (residues 343:356, 372:395, 425:444, 468:513; force constant = 20 kcal/mol Å^2). In each round of model building, a combination of σ_A weighted[47] $2|F_o|-|F_c|$ and $|F_o|-|F_c|$ maps (calculated with model phases combined with experimental phases or model phases alone) and simulated annealing omit maps[48] were used. B-factor sharpening of the observed diffraction data improved electron density maps and allowed for visualization of more side-chain details.[49,50] The formula used for applying B-factor sharpening to the observed structure factors is:

$$F_{sharp}(s) = F_{obs}/\exp(-2B_{sharp}(\sin\theta/\lambda)^2)$$

The optimum value of 20 Å^2 for B_{sharp} was obtained by observing improvements in the electron density maps.

The structure of the longer construct (residues 63–623), from data obtained from selenomethionine substituted protein crystals, was solved by molecular replacement. The refined dimer of the 63–524 construct was used as a search model using the program MOLREP.[51] Placement of the first dimer gave an R value of 60.1% and a correlation coefficient of 19.6%. Placement of the second dimer improved the R value to 58.7% and the correlation

coefficient to 23.8%. Rigid body refinement resulted in an R_{free} of 52.5%. The solution was confirmed by calculating an anomalous Fourier map to check for the positions of the known selenomethionine residues. Phases from the model were used to calculate a σ_A weighted[47] electron density map to 3.5 Å. This map was improved by solvent flattening and fourfold NCS averaging using DM.[52] Two masks per protomer were used; mask 1 for residues 74:341 and mask 2 for residues 342:513. This new map allowed tracing of the last 100 residues of Exo70p. The model was further refined using CNS as described above.[53] Separate NCS restraints were applied to two parts of the molecule, one for residues 74:341 and the other for residues 342:623; a strong force constant of 300 kcal/mol Å^2 was applied in order to prevent significant variations amongst the different NCS-related molecules. During each round of rebuilding, one molecule was rebuilt and then transformed using the two NCS operators to generate the other three molecules in the asymmetric unit, so that two-domain, fourfold NCS restraints could be imposed. With the restraints set at 300 kcal/mol Å^2 the molecules were kept nearly identical during refinement but the two separate domains were able to move separately.

The final model includes residues 73–223, 236–527, 544–623. The overall *B* factor for chain A is 100 Å^2, for chain B is 138 Å^2, for chain C is 148 Å^2 and for chain D is 134 Å^2. Ramachandran plot statistics (Table 1) are as defined by PROCHECK.[54] Figures were generated using MOLSCRIPT[55] and RASTER-3D.[56] Molecular surfaces were generated using ProtSkin[57] and PYMOL.[58] Surface potentials were calculated using APBS.[59] Buried surface areas were calculated using CNS[53] with a 1.4 Å probe radius.

Surface plasmon resonance measurements

The binding constants for the interaction between Exo70p and Rho3p were obtained from surface plasmon resonance (SPR) measurements, performed on a BIAcore 2000 instrument. Exo70p constructs containing residues 1–623 (465 RUs), 63–623 (387 RUs) and 63–524 (1417 RUs) were immobilized on a reagent-grade CM5 sensor chip (Biacore) using primary amine coupling as described in the BIAcore manual. To subtract background the first flow cell was mock coupled with buffer only. A twofold concentration series from 0.39 μM to 200 μM of Rho3p-Q74L (lacking the CAAX box) was injected over the surface of the chip at 50 μl/min in 50 mM Hepes (pH 7.5), 300 mM NaCl, 10 mM $MgCl_2$, 2 mM DTT, 0.005% (v/v) P20, 0.5 mM GTP. The sensorgrams were processed using the BIAevaluation software (Biacore). Equilibrium dissociation constants (K_Ds) were derived by non-linear regression analysis of plots of R_{eq} (equilibrium binding response) *versus* the log of the injected protein concentration. The data were fit to a simple 1:1 binding model.

To determine if the binding interaction is dependent on GTP, Exo70p construct containing residues 63–623 was coupled to a CM5 sensor chip at a density of 1144 RUs. 100 μl of the WT-Rho3p (lacking the CAAX box) at 40 μM concentration was injected over the chip at 50 μl/min in 50 mM Hepes (pH 7.5), 300 mM NaCl, 10 mM $MgCl_2$, 2 mM DTT, 0.005% (v/v) P20 and 0.5 mM GTP or 0.5 mM GDP.

Protein Data Bank accession number

Atomic coordinates and structure factors have been deposited in the RCSB Protein Data Bank with accession code 2B7M.

Acknowledgements

We thank the staff at SSRL and the ALS for assistance with data collection; Patrick Brennwald and Hao Wu for sharing unpublished data; Doug Hattendorf for carefully reading this manuscript; and Pamela J. Bjorkman for providing access to the BIAcore instrument. Portions of this research were carried out at the Stanford Synchrotron Radiation Laboratory, a national user facility operated by Stanford University on behalf of the U.S. Department of Energy, Office of Basic Energy Sciences. The SSRL Structural Molecular Biology Program is supported by the Department of Energy, Office of Biological and Environmental Research, and by the National Institutes of Health, National Center for Research Resources, Biomedical Technology Program, and the National Institute of General Medical Sciences. The Advanced Light Source is supported by the Director, Office of Science, Office of Basic Energy Sciences, of the U.S. Department of Energy under Contract No. DE-AC02-05CH11231. Z.A.H. is supported by a fellowship from the Damon Runyon Cancer Research Foundation (DRG-1772-03). A.E.H. and A.P.W. are supported by grants R01 DK60770-01 and R37 AI041239 to P. J. Bjorkman from the National Institutes of Health. This work was supported by grant MH58570 from the National Institutes of Health to W.I.W.

References

1. TerBush, D. R., Maurice, T., Roth, D. & Novick, P. (1996). The Exocyst is a multiprotein complex required for exocytosis in *Saccharomyces cerevisiae*. *EMBO J.* **15**, 6483–6494.
2. Grindstaff, K. K., Yeaman, C., Anandasabapathy, N., Hsu, S. C., Rodriguez-Boulan, E., Scheller, R. H. & Nelson, W. J. (1998). Sec6/8 complex is recruited to cell–cell contacts and specifies transport vesicle delivery to the basal–lateral membrane in epithelial cells. *Cell*, **93**, 731–740.
3. Finger, F. P., Hughes, T. E. & Novick, P. (1998). Sec3p is a spatial landmark for polarized secretion in budding yeast. *Cell*, **92**, 559–571.
4. Novick, P., Field, C. & Schekman, R. (1980). Identification of 23 complementation groups required for post-translational events in the yeast secretory pathway. *Cell*, **21**, 205–215.
5. Guo, W., Grant, A. & Novick, P. (1999). Exo84p is an exocyst protein essential for secretion. *J. Biol. Chem.* **274**, 23558–23564.
6. Sivaram, M. V., Saporita, J. A., Furgason, M. L., Boettcher, A. J. & Munson, M. (2005). Dimerization of the exocyst protein Sec6p and its interaction with the t-SNARE Sec9p. *Biochemistry*, **44**, 6302–6311.
7. Zhang, X., Wang, P., Gangar, A., Zhang, J., Brennwald, P., Terbush, D. & Guo, W. (2005). Lethal giant larvae proteins interact with the exocyst complex and are involved in polarized exocytosis. *J. Cell Biol.* **170**, 273–283.
8. Brennwald, P., Kearns, B., Champion, K., Keranen, S., Bankaitis, V. & Novick, P. (1994). Sec9 is a SNAP-25-

like component of a yeast SNARE complex that may be the effector of Sec4 function in exocytosis. *Cell*, **79**, 245–258.
9. Finger, F. P. & Novick, P. (1997). Sec3p is involved in secretion and morphogenesis in *Saccharomyces cerevisiae*. *Mol. Biol. Cell*, **8**, 647–662.
10. Mondesert, G., Clarke, D. J. & Reed, S. I. (1997). Identification of genes controlling growth polarity in the budding yeast *Saccharomyces cerevisiae*: a possible role of *N*-glycosylation and involvement of the exocyst complex. *Genetics*, **147**, 421–434.
11. Haarer, B. K., Corbett, A., Kweon, Y., Petzold, A. S., Silver, P. & Brown, S. S. (1996). SEC3 mutations are synthetically lethal with profilin mutations and cause defects in diploid-specific bud-site selection. *Genetics*, **144**, 495–510.
12. Sugihara, K., Asano, S., Tanaka, K., Iwamatsu, A., Okawa, K. & Ohta, Y. (2002). The exocyst complex binds the small GTPase RalA to mediate filopodia formation. *Nature Cell Biol.* **4**, 73–78.
13. Wang, S., Liu, Y., Adamson, C. L., Valdez, G., Guo, W. & Hsu, S. C. (2004). The mammalian exocyst, a complex required for exocytosis, inhibits tubulin polymerization. *J. Biol. Chem.* **279**, 35958–35966.
14. Lipschutz, J. H., Lingappa, V. R. & Mostov, K. E. (2003). The exocyst affects protein synthesis by acting on the translocation machinery of the endoplasmic reticulum. *J. Biol. Chem.* **278**, 20954–20960.
15. Awasthi, S., Palmer, R., Castro, M., Mobarak, C. D. & Ruby, S. W. (2001). New roles for the Snp1 and Exo84 proteins in yeast pre-mRNA splicing. *J. Biol. Chem.* **276**, 31004–31015.
16. Novick, P. & Guo, W. (2002). Ras family therapy: Rab, Rho and Ral talk to the exocyst. *Trends Cell Biol.* **12**, 247–249.
17. Lipschutz, J. H. & Mostov, K. E. (2002). Exocytosis: the many masters of the exocyst. *Curr. Biol.* **12**, R212–R214.
18. Robinson, N. G., Guo, L., Imai, J., Toh, E. A., Matsui, Y. & Tamanoi, F. (1999). Rho3 of *Saccharomyces cerevisiae*, which regulates the actin cytoskeleton and exocytosis, is a GTPase which interacts with Myo2 and Exo70. *Mol. Cell. Biol.* **19**, 3580–3587.
19. Adamo, J. E., Rossi, G. & Brennwald, P. (1999). The Rho GTPase Rho3 has a direct role in exocytosis that is distinct from its role in actin polarity. *Mol. Biol. Cell*, **10**, 4121–4133.
20. Zhang, X., Bi, E., Novick, P., Du, L., Kozminski, K. G., Lipschutz, J. H. & Guo, W. (2001). Cdc42 interacts with the exocyst and regulates polarized secretion. *J. Biol. Chem.* **276**, 46745–46750.
21. Guo, W., Roth, D., Walch-Solimena, C. & Novick, P. (1999). The exocyst is an effector for Sec4p, targeting secretory vesicles to sites of exocytosis. *EMBO J.* **18**, 1071–1080.
22. Moskalenko, S., Tong, C., Rosse, C., Mirey, G., Formstecher, E., Daviet, L. *et al*. (2003). Ral GTPases regulate exocyst assembly through dual subunit interactions. *J. Biol. Chem.* **278**, 51743–51748.
23. Moskalenko, S., Henry, D. O., Rosse, C., Mirey, G., Camonis, J. H. & White, M. A. (2002). The exocyst is a Ral effector complex. *Nature Cell Biol.* **4**, 66–72.
24. Jin, R., Junutula, J. R., Matern, H. T., Ervin, K. E., Scheller, R. H. & Brunger, A. T. (2005). Exo84 and Sec5 are competitive regulatory Sec6/8 effectors to the RalA GTPase. *EMBO J.* **24**, 12.
25. Inoue, M., Chang, L., Hwang, J., Chiang, S. H. & Saltiel, A. R. (2003). The exocyst complex is required for targeting of Glut4 to the plasma membrane by insulin. *Nature*, **422**, 629–633.
26. Lipschutz, J. H., Guo, W., O'Brien, L. E., Nguyen, Y. H., Novick, P. & Mostov, K. E. (2000). Exocyst is involved in cystogenesis and tubulogenesis and acts by modulating synthesis and delivery of basolateral plasma membrane and secretory proteins. *Mol. Biol. Cell*, **11**, 4259–4275.
27. Yeaman, C., Grindstaff, K. K., Wright, J. R. & Nelson, W. J. (2001). Sec6/8 complexes on trans-Golgi network and plasma membrane regulate late stages of exocytosis in mammalian cells. *J. Cell Biol.* **155**, 593–604.
28. Prigent, M., Dubois, T., Raposo, G., Derrien, V., Tenza, D., Rosse, C. *et al*. (2003). ARF6 controls post-endocytic recycling through its downstream exocyst complex effector. *J. Cell Biol.* **163**, 1111–1121.
29. Murthy, M., Ranjan, R., Denef, N., Higashi, M. E., Schupbach, T. & Schwarz, T. L. (2005). Sec6 mutations and the *Drosophila* exocyst complex. *J. Cell Sci.* **118**, 1139–1150.
30. Bowser, R. & Novick, P. (1991). Sec15 protein, an essential component of the exocytotic apparatus, is associated with the plasma membrane and with a soluble 19.5 S particle. *J. Cell Biol.* **112**, 1117–1131.
31. Guo, W., Tamanoi, F. & Novick, P. (2001). Spatial regulation of the exocyst complex by Rho1 GTPase. *Nature Cell Biol.* **3**, 353–360.
32. Matern, H. T., Yeaman, C., Nelson, W. J. & Scheller, R. H. (2001). The Sec6/8 complex in mammalian cells: characterization of mammalian Sec3, subunit interactions, and expression of subunits in polarized cells. *Proc. Natl Acad. Sci. USA*, **98**, 9648–9653.
33. Wang, H., Tang, X. & Balasubramanian, M. K. (2003). Rho3p regulates cell separation by modulating exocyst function in *Schizosaccharomyces pombe*. *Genetics*, **164**, 1323–1331.
34. Xu, K. F., Shen, X., Li, H., Pacheco-Rodriguez, G., Moss, J. & Vaughan, M. (2005). Interaction of BIG2, a brefeldin A-inhibited guanine nucleotide-exchange protein, with exocyst protein Exo70. *Proc. Natl Acad. Sci. USA*, **102**, 2784–2789.
35. Holm, L. & Sander, C. (1998). Protein folds and families: sequence and structure alignments. *Nucl. Acids Res.* **26**, 316–319.
36. Janin, J. (1997). Specific *versus* non-specific contacts in protein crystals. *Nature Struct. Biol.* **4**, 973–974.
37. Imamura, H., Tanaka, K., Hihara, T., Umikawa, M., Kamei, T., Takahashi, K. *et al*. (1997). Bni1p and Bnr1p: downstream targets of the Rho family small G-proteins which interact with profilin and regulate actin cytoskeleton in *Saccharomyces cerevisiae*. *EMBO J.* **16**, 2745–2755.
38. May, A. P., Misura, K. M., Whiteheart, S. W. & Weis, W. I. (1999). Crystal structure of the amino-terminal domain of *N*-ethylmaleimide-sensitive fusion protein. *Nature Cell Biol.* **1**, 175–182.
39. Otwinowski, Z. & Minor, W. (1997). Processing of X-ray diffraction data collected in oscillation mode. *Methods Enzymol.* **276**, 307–326.
40. Terwilliger, T. C. & Berendzen, J. (1999). Automated MAD and MIR structure solution. *Acta Crystallog. sect. D*, **55**, 849–861.
41. De La Fortelle, E. & Bricogne, G. (1997). Maximum-likelihood heavy-atom parameter refinement for

multiple isomorpous replacement and multiwavelength anomalous diffraction methods. *Methods Enzymol.* **276**, 472–494.
42. Abrahams, J. P. & Leslie, A. G. W. (1996). Methods used in the structure determination of bovine mitochondrial F1 ATPase. *Acta Crystallog. sect. D*, **52**, 30–42.
43. Kleywegt, G. J. & Jones, T. A. (1997). Template convolution to enhance or detect structural features in macromolecular electron-density maps. *Acta Crystallog. sect. D*, **53**, 179–185.
44. Jones, T. A. & Kjeldgaard, M. (1997). Electron density map interpretation. *Methods Enzymol.* **277**, 173–208.
45. Brunger, A. T., Adams, P. D., Clore, G. M., Delano, W. L., Gros, P., Grosse-Kunstleve, R. W. *et al.* (1998). Crystallography & NMR system: a new software suite for macromolecular structure determination. *Acta Crystallog. sect. D*, **54**, 905–921.
46. Kleywegt, G. J. & Jones, T. A. (1996). xdlMAPMAN and xdlDATAMAN—programs for reformatting, analysis and manipulation of biomacromolecular electron-density maps and reflection data sets. *Acta Crystallog. sect. D*, **52**, 826–828.
47. Read, R. J. (1986). Improved Fourier coefficients for maps using phases from partial structures with errors. *Acta Crystallog. sect. A*, **42**, 140–149.
48. Hodel, A., Kim, S.-H. & Brünger, A. T. (1992). Model bias in macromolecular crystal structures. *Acta Crystallog. sect. A*, **48**, 851–858.
49. Bass, R. B., Strop, P., Barclay, M. & Rees, D. C. (2002). Crystal structure of *Escherichia coli* MscS, a voltage-modulated and mechanosensitive channel. *Science*, **298**, 1582–1587.
50. DeLaBarre, B. & Brunger, A. T. (2003). Complete structure of p97/valosin-containing protein reveals communication between nucleotide domains. *Nature Struct. Biol.* **10**, 856–863.
51. Vagin, A. & Teplyakov, A. (1997). MOLREP: an automated program for molecular replacement. *J. Appl. Crystallog.* **30**, 1022–1025.
52. Cowtan, K. (1994). dm: an automated procedure for phase improvement by density modification. In: *Joint CCP4 and ESF-EACBM Newsletter on Protein Crystallography*, **31**, 34–38.
53. Brünger, A. T., Adams, P. D., Clore, G. M., Gros, P., Grosse-Kunstleve, R. W., Jiang, J.-S. *et al.* (1998). Crystallography and NMR system: a new software system for macromolecular structure determination. *Acta Crystallog. sect. D*, **54**, 905–921.
54. Laskowski, R. A., MacArthur, M. W., Moss, D. S. & Thornton, J. M. (1993). PROCHECK: a program to check the stereochemical quality of protein structures. *J. Appl. Crystallog.* **26**, 283–291.
55. Kraulis, P. (1991). MOLSCRIPT: a program to produce both detailed and schematic plots of protein structures. *J. Appl. Crystallog.* **24**, 946–950.
56. Merritt, E. A. & Bacon, D. J. (1997). Raster3D: photorealistic molecular graphics. *Methods Enzymol.* **277**, 505–524.
57. Deprez, C., Lloubes, R., Gavioli, M., Marion, D., Guerlesquin, F. & Blanchard, L. (2005). Solution structure of the *E. coli* TolA C-terminal domain reveals conformational changes upon binding to the phage g3p N-terminal domain. *J. Mol. Biol.* **346**, 1047–1057.
58. DeLano, W. L. (2002). *The PyMOL Moleculare Graphics System*, DeLano Scientific, San Carlos, CA, USA.
59. Baker, N. A., Sept, D., Joseph, S., Holst, M. J. & McCammon, J. A. (2001). Electrostatics of nanosystems: application to microtubules and the ribosome. *Proc. Natl Acad. Sci. USA*, **98**, 10037–10041.
60. Jeanmougin, F., Thompson, J. D., Gouy, M., Higgins, D. G. & Gibson, T. J. (1998). Multiple sequence alignment with Clustal X. *Trends Biochem. Sci.* **23**, 403–405.
61. Brünger, A. T. (1992). Free *R* value: a novel statistical quantity for assessing the accuracy of crystal structures. *Nature*, **355**, 472–475.

Edited by R. Huber

(Received 2 August 2005; accepted 29 September 2005)
Available online 10 November 2005

Note added in proof: After the submission of this manuscript, the structure of the C-terminal region of Sec15, another exocyst component, was reported (Wu *et al.*, *Nature Struct. Mol. Biol.* Sept 11, 2005, epub ahead of print). The topology of helices in the C-terminal region of Sec15 is similar to that of Exo70p domains D1 and D2, although relative positions of the two subdomains differ in the two proteins. The observation that a region of Exo70p has a similar fold to that of the C-terminal region of Sec15 is surprising and may suggest divergent evolution from a common fold.